Formation and Stability of Shear-Induced Shish-Kebab Structure in Highly Entangled Melts of UHMWPE/HDPE Blends

Jong Kahk Keum, Feng Zuo, and Benjamin S. Hsiao*

Department of Chemistry, Stony Brook University, Stony Brook, New York 11794-3400

Received January 10, 2008; Revised Manuscript Received April 21, 2008

ABSTRACT: The formation and stability of a shear-induced shish-kebab structure was investigated by in situ rheo-SAXS (small-angle X-ray scattering) and -WAXD (wide-angle X-ray diffraction) measurements of highly entangled polyethylene melts based on two polymer blends, containing small fractions (2 and 5 wt %) of ultra-high molecular weight polyethylene (UHMWPE) and high-density polyethylene (HDPE). Immediately after shear, the combined SAXS and WAXD results at 142 °C confirmed the sole formation of shish without kebabs, indicating the interplay between the topological deformation of highly entangled UHMWPE chains and the extended-chain crystallization of stretched segments without the participation of coiled segments. The presence of HDPE chains influenced the entanglement of UHMWPE but they were not involved in the shish-kebab formation at the initial stage of crystallization. The final shish lengths in both blends were nearly identical at the same strain ($\varepsilon = 500$), even though the UHMWPE concentration was different. When the temperature was cooled to 134 °C, both sheared blends exhibited the kebab formation, following the diffusion-controlled growth process. Although the total kebab nucleation was higher in the 5/95 wt % UHMWPE/HDPE blend, the kebab density per shish was higher in the 2/98 wt % UHMWPE/HDPE blend. The thermal stability of the shish-kebab structure was also investigated by constrained melting. Both blends exhibited identical melting behavior of kebabs but different melting behavior of shish that is governed by the entanglement restraints of the stretched-chain network.

Introduction

Flow-induced crystallization of semicrystalline polymers is an important subject with many practical implications from process design to property control. In particular, the molecular mechanism responsible for the initial formation of the "precursor structure" under flow prior to full scale crystallization in highly entangled polymer melts is of great interest to both academic and industrial communities.[1–14] The current thinking considers that deformation of highly entangled species in the melt directly results in extended-chain crystallization forming shish and subsequent folded-chain crystallization forming kebabs, and thus indirectly influences the final morphology of polymer products.[12] However, the experimental results revealing the kinetic evolution and thermal stability of flow-induced shish-kebab structure are rare, which is the purpose of this study.

Recently, in situ rheo-X-ray studies confirmed that the high molecular weight species play an essential role in forming the initial crystallization precursor structure (shish-kebabs) in the entangled melt under a given flow condition.[10–17] The molecular basis of flow-induced shish-kebab formation in entangled polymer melt has been related to the concept of a coil−stretch transition for polymer chains, which was first proposed by de Gennes decades ago based on the chain dynamics in dilute solutions.[18] Later, Chu et al. experimentally verified that the coil−stretch transition of a single DNA chain in dilute solution is indeed the first-order transition, where the conformation change occurs abruptly above a critical strain rate, $\dot{\epsilon}_c$.[19] For flow-induced crystallization in entangled polymer melts, Keller also adopted the concept of coil-stretch transition. He proposed the existence of a critical orientation molecular weight, M^*, for linear polymer chains, which can be scaled with critical strain $\dot{\epsilon}_c \sim (M^*)^{-\beta}$.[20] Thus, only the polymer chains with molecular weights higher than M^*can remain stretched after a given flow, while shorter chains relax back to the coiled state. However, the coil−stretch transition at the whole chain level in entangled melt is still a controversial viewpoint. This is because it is very unlikely that a long entangled chain can disentangle itself and undergo the stretch−coil transition under typical experimental conditions, as in our recent rheo-X-ray studies.[12]

Different from the concept of Keller et al.,[20] we hypothesize that the deformation of highly entangled chains in a supercooled state can produce a stable oriented network of entangled chains, consisting of stretched segments and coiled segments between the "frozen" entanglement points similar to network materials containing (physical or chemical) cross-linking points. The process may not need to undergo the stretch-coil transition. The stretched segments can undergo extended-chain crystallization and form shish, where the coiled segment can subsequently undergo folded-chain crystallization and form kebabs.[12] The interplay between the flow field and the chain dynamics of the high molecular weight species in particular shall thus dictate the topology of the flow-induced shish-kebab scaffold. The concept of M^* for entangled melt is still valid and useful, but the clear definition of M^* and the appropriate methodology to determine its value still requires further investigation.

In our previous studies,[21] a bimodal blend containing a small fraction of crystallizing high molecular species in the matrix of noncrystallizing lower molecular weight species was used as a model system to investigate the formation of precursor structure (shish-kebabs) induced by flow before full scale crystallization. It has been demonstrated that the phase separation in bimodal polymer blends containing identical chemical composition (i.e., the interaction parameter χ is near zero) but different chain length or chain branching (i.e., different relaxation time spectrum and viscosities) can be induced by flow.[22,23] In fact, the miscibility between the two species depends on the strength of the flow field. Under strong flow (e.g., fiber spinning and injection molding), large phase separated domains (in micrometers), such as microfibrillar superstructure or even larger skin-core morphology, can be produced. Under weak flow (as in this study), nanoscopic phase separated domains (in tens of nanometers) can be obtained. The former may be dominated by the behavior of large scale liquid−liquid phase separation (LLPS)[24], while the latter may be dominated by the process of crystal-

* To whom correspondence should be addressed. E-mail: bhsiao@notes.cc.sunysb.edu. Telephone: 631-632-7793. Fax: 631-632-6518.

10.1021/ma800063e CCC: $40.75
Published on Web 06/12/2008

lization from oriented chains. Recently, Olmsted et al. have rationalized the occurrence of nanoscopic liquid−liquid phase separation in polymer melt prior to crystallization through the pathway of spinodal decomposition, even in the absence of flow.[24] However, we do not feel that the step of spinodal decomposition is necessary to induce the shish-kebab structure by flow.

A great deal of effort has been made to understand the nucleation and growth behavior of polymers under flow in the last several decades. The general behavior of flow-induced crystallization can be understood by conventional theories,[20] and the kinetics process can only be approximately described by phenomenological expressions.[25] However, the exact molecular mechanism responsible for the nucleation and growth processes at the very initial stage under flow is still unclear. Thus, in this study, our main objective is to elucidate the molecular nature of flow-induced crystallization precursor structures in entangled polymer melts. In order to carry out the study properly, the choice of suitable samples and the design of appropriate experimental conditions were carefully made. For sample selection, two linear polyethylene (PE) samples with very different average molecular weights: high density polyethylene, HDPE, (M_w= 112 000 g/mol) and ultra high molecular weight polyethylene, UHMWPE (M_w = 5 000 000−6 000 000 g/mol) were chosen. The former was used as a matrix and the latter (in small fractions) was used as precursor forming species (a similar study using a lower molecular weight PE (M_w = 50 000 g/mol, polydispersity = 2.1) as the matrix has been carried out by us previously[21]). The experimental temperature was selected to be above the melting point of HDPE, where only the crystallization behavior of UHMWPE could be observed. Furthermore, the experimental temperature was first set sufficiently high only to allow the real-time investigation of shish formation, but not kebab formation, using in situ small-angle X-ray scattering (SAXS) and wide-angle X-ray diffraction (WAXD) techniques with synchrotron radiation.

Experimental Section

Materials and Sample Preparation. The HDPE sample (M_w= 112,000 g/mol, polydispersity ∼ 9.1) was provided by the Dow Chemical Company; the UHMWPE sample (M_w=5 000 000−6 000 000 g/mol, polydispersity ∼ 9.0) was provided by Basell USA. Both samples were polymerized by Ziegler−Natta catalysts and had broad polydispersity. The chosen concentrations of UHMWPE in the two blends were 2 and 5 wt % (we termed these 2/98 and 5/95 blends, respectively), which were significantly higher than the estimated overlap concentration of UHMWPE (c^* ∼ 0.2 wt %). The overlap concentration was estimated based on the equation $c^* = 3M_w/4\pi[\langle R^2_g\rangle^{1/2}]^3N_a$, with $\langle R^2_g\rangle^{1/2}$ being the root-mean-square radius of gyration and N_a being Avogadro's number.[21,26,27] The characteristic ratio of $\langle R^2_g\rangle^{1/2}M_w^{1/2}$ for PE was 0.46, based on SANS measurements.[28]

The polymer blends were prepared by a solution blending procedure to ensure that the two species were intimately mixed at the molecular level. In order to prevent the sample degradation during mixing, 3 wt % of antioxidants (Irgonox 1076) was added. The detailed mixing procedure has been described elsewhere.[21] A control sample of neat HDPE without the addition of UHMWPE was also prepared using the same procedure. Polymer films with about 0.5 mm thickness were prepared by compression molding at 172 °C for 5 min. Samples in the form of a ring (inner diameter = 10 mm; outer diameter = 20 mm) were cut from the melt pressed films for rheo-X-ray measurements.

Instrumentation. A Linkam CSS-450 optical shear stage, modified for in situ rheo-X-ray experiments was used to apply controlled step shear to the blend samples. The details of this modified shear apparatus have been described elsewhere.[14] In short, the sample was placed in the gap between two X-ray windows (i.e., a Kapton window and a diamond window) and was completely enclosed in the measuring cell. The chosen step shear conditions were as follows: shear rate $\dot{\gamma} = 100\ s^{-1}$ and duration time $t_s = 5$ s, where a constant strain (ϵ) of 500 shear units was applied to the samples.

In situ rheo-SAXS (small-angle X-ray scattering) and rheo-WAXD (wide-angle X-ray diffraction) measurements were carried out at the X27C beamline in the National Synchrotron Light Source (NSLS), Brookhaven National Laboratory (BNL). The X-ray wavelength was 1.371 Å. Two dimensional (2D) SAXS and WAXD patterns were collected by using a MAR CCD X-ray detector (MAR-USA), which had a resolution of 1024 × 1024 pixels (pixel size = 158.44 μm). For SAXS measurements, the sample-to-detector distance was 1832 mm and the scattering angle was calibrated by silver behenate (AgBe). For WAXD measurements, the sample-to-detector distance was 112.4 mm and the diffraction angle was calibrated by aluminum oxide (Al_2O_3). All X-ray images (SAXS and WAXD) were corrected for background scattering, air scattering, sample absorption and synchrotron X-ray beam fluctuations.

Experimental Procedures. In order to ensure that the melts were free of any memory effects associated with prior thermal and mechanical histories, all samples were first heated to 172 °C, which was substantially higher than the equilibrium melting temperature for PE ($T_m° \approx 145.5$ °C), for 5 min. The melts were then rapidly cooled to the chosen crystallization temperature (i.e., 142 °C) at a −30 °C/min rate for in situ SAXS and WAXD measurements. As the programmed temperature reached the crystallization temperature (i.e., 142 °C), the sample was equilibrated for 2 min before the application of shear to ensure that the true sample temperature reached the preset value of 142 °C. Then a shear was applied to samples with a shear rate of $\gamma = 100\ s^{-1}$ for 5 s. The data acquisition time was 15 s and the data storage time was 5 s for each SAXS and WAXD image collection. After 45 min of isothermal measurement, the once-sheared melt was subsequently cooled to 134 °C and held there for 30 min to study further crystallization. The resulting once-sheared and crystallized sample was then gradually heated from 134 °C to above the melting point at a rate of 1 °C/min under confined planar restraint in the shear stage to examine the thermal stability of the shear-induced shish-kebab structure.

Results and Discussion

Flow-Induced Shish Formation (without Kebabs) at T_c = 142 °C. Figure 1 illustrates selected 2D SAXS patterns for each PE blend (2 and 5 wt %) collected at varying times before and after step shear $\gamma = 100\ s^{-1}$ and shear duration $t_s = 5$ s) at 142 °C; Before shear, all three samples exhibited only diffused scattering features, typical of PE melts without ordered structure and preferred orientation. Immediately after shear, however, strong equatorial streaks appeared in both blends, as indicated by arrows in parts b and c of Figure 1. The appearance of the equatorial streak is consistent with the formation of shish (we speculate that it may be related to the formation of multiple shish instead of single shish[10]) having strong electron density contrast between the shish and the surrounding molten matrix.

Figure 2 shows selected 2D WAXD patterns of three samples (neat HDPE and two blends) collected before and after shear under the same shearing conditions as those in rheo-SAXS measurements. It was seen that highly oriented equatorial (110) reflection peaks appeared in the blend samples immediately after shear (Figure 2, parts b and c), implying that the formation of shish consisted of highly oriented crystals probably with extended-chain conformation. In contrast, the neat HDPE melt did not show any sign of shish formation by both SAXS and WAXD after shear (Figures 1a and 2a, respectively). We note that SAXS is insensitive to the scatterer with low concentration or with low electron density contrast, thus the absence of equatorial streak in SAXS does not necessarily mean the absence of shish. However, the results from subsequent crystallization at lower temperatures (i.e., 137 and 131 °C), which will be

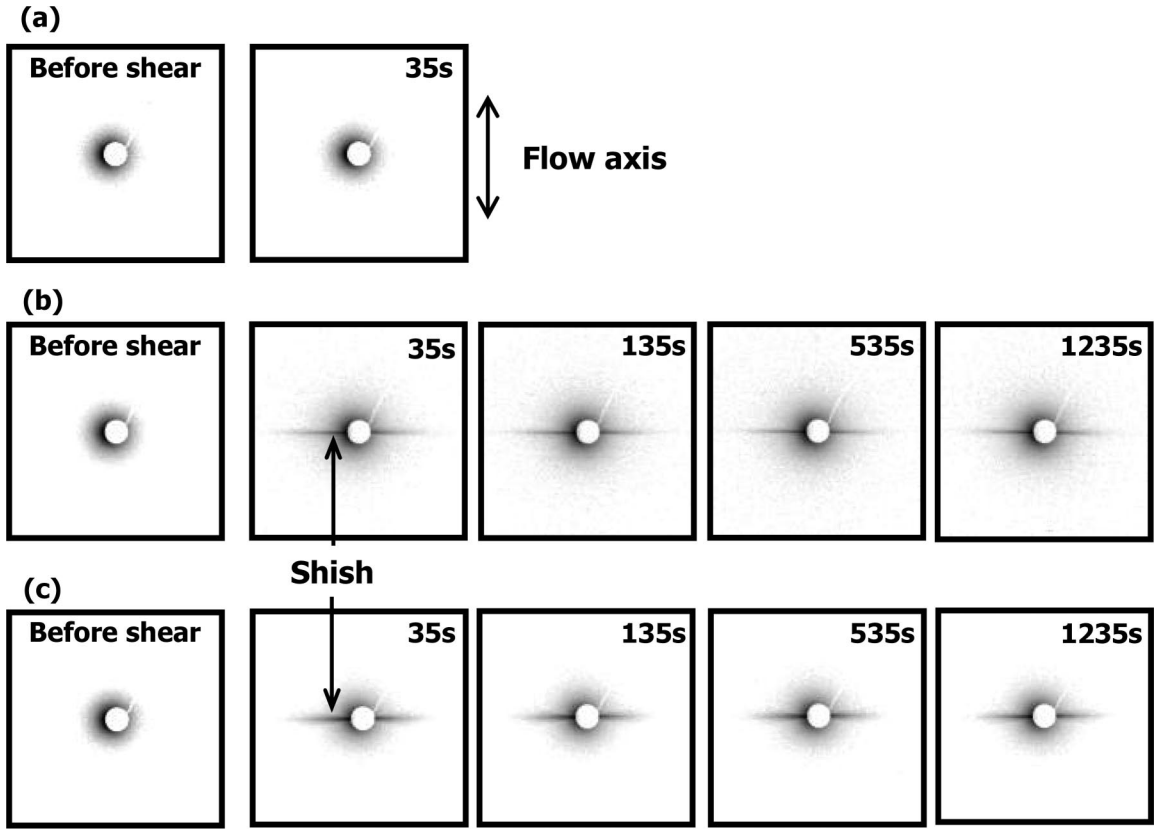

Figure 1. Selected rheo-SAXS patterns of (a) neat HDPE, (b) 2/98 wt % UHMWPE/HDPE blend, and (c) 5/95 wt % UHMWPE/HDPE blend. Each SAXS pattern was collected at different times before and after step shear (rate $\dot{\gamma} = 100\ s^{-1}$, shear duration $t_s = 5$ s) and at 142 °C.

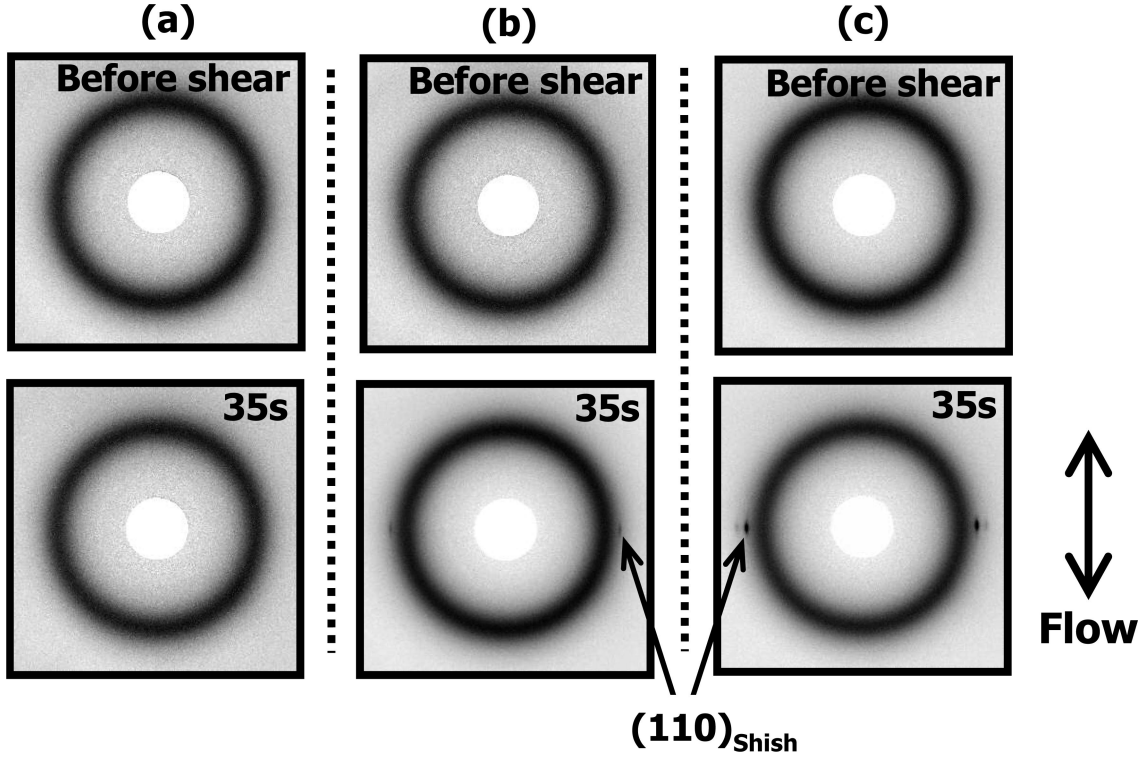

Figure 2. Selected rheo-WAXD patterns of (a) neat HDPE, (b) 2/98 wt % UHMWPE/HDPE blend, and (c) 5/95 wt % UHMWPE/HDPE blend obtained before and after the step shear at 142 °C ($\dot{\gamma} = 100\ s^{-1}$ and $t_s = 5$ s).

discussed later, confirmed that the shish were not formed in the sheared HDPE melt at 142 °C since WAXD only exhibited an amorphous scattering feature and SAXS indicated completely unoriented lamellar scattering. In other words, the experimental temperature (142 °C) was sufficiently high to prevent the long chain species in HDPE to sustain the stretched and oriented state under shear.

The appearance of equatorial streak in SAXS and a pair of equatorial (110) reflections in WAXD from the blend samples can be directly attributed to the crystallization of sheared

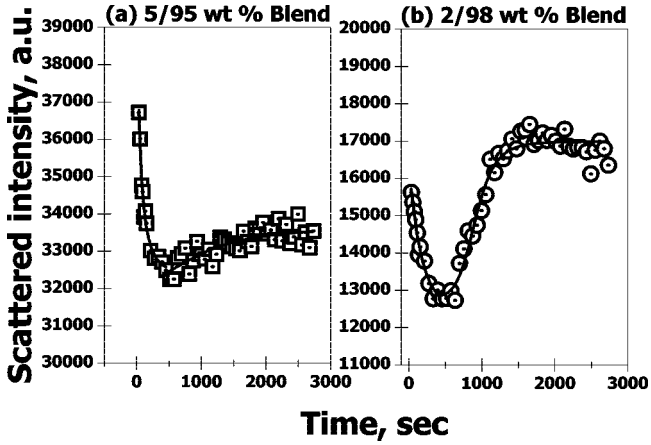

Figure 3. Changes of the scattered intensity from shish in (a) 5/95 wt % UHMWPE/HDPE blend and (b) 2/98 wt % UHMWPE/HDPE blend. The scattered intensity of shish (I_{shish}) was extracted from 2D rheo-SAXS patterns which were partially illustrated in Figure 1, parts b and c.

UHMWPE component. Since the concentrations of UHMWPE in both blends were significantly higher than the overlap concentration, c^*, all UHMWPE chains could remain stretched and oriented after shear (although the degrees of extension and orientation were a function of position along the gradient direction, i.e., the sample thickness). This is because the relaxation time, τ, of the polymer chain is scaled with its molecular weight, M, where $\tau \sim M^{3.4}$, where the average relaxation time of UHMWPE chains is an order of magnitude higher than that of HDPE.

It is interesting to note that, even though both blends exhibited the formation of shish, the signature of kebab formation, such as the emergence of meridional scattering maxima in SAXS, was not seen. This indicates that the chosen experimental temperature only allowed the formation of shish (with a higher melting point) but hindered the formation of kebabs (with a lower melting point) in UHMWPE. In our previous studies, the kebab formation took place at the same time scale, almost immediately after the appearance of shish.[10,11,14,21] The short separation time between the formation of shish and kebabs implied that the nucleation barrier of kebabs at the shish/melt interface was relatively low at lower experimental temperatures. Muthukumar et al. proposed that the nucleation of kebab from the presence of shish involves the adsorption of coiled-chain segments through a diffusion process.[9] It is thus reasonable to argue that when the temperature is high (e.g., close to the equilibrium melting temperature), the mobility of the chain segments may be too high to be adsorbed and stay anchored on the shish. The absence of kebab formation at the chosen experimental temperature (142 °C) thus can be attributed to the sufficiently high temperature, where coiled-chain segments cannot overcome the secondary nucleation barrier to form folded-chain lamellar crystal.

Although no kebab was formed at 142 °C after shear, the shish was found to first relax and then subsequently grow in both blends during isothermal conditions after shear. To illustrate this unique behavior, the scattered intensity of shish, I_{shish}, extracted from the 2D SAXS pattern using the expression

$$I_{shish} = 4\pi \int_{0.0087}^{0.31} \int_{0^\circ}^{20^\circ} I(s,\phi)\, ds\, d\phi \qquad (0)$$

(s is the scattering vector, where $s = 2(\sin\theta)/\lambda$, with θ being the scattering angle and λ being the X-ray wavelength, and ϕ is the azimuthal angle) as a function of crystallization time is shown in Figure 3. The observed scattered intensity changes in different blends exhibited a similar trend, which could be divided into two stages: the initial decrease at $t \sim 400$ s and the later increase at $t \sim 400$ s; in which a minimum value was seen. The 5/95 blend exhibited notably higher scattered intensity than the 2/98 blend during the entire crystallization stage at 142 °C after shear. Since the scattered intensity, $I_{shish}(s, \phi)$, is proportional to the volume of shish, v, as well as the density contrast between the shish and surrounding matrix, $\Delta\rho$, it can be thought that higher volume fraction of shish or more closely packed shish was formed in the 5/95 blend than that in the 2/98 blend. This behavior is certainly consistent with the notation that only the UHMWPE component has crystallized in the blends under the experimental conditions, where the 5/95 blend would result in higher scattered intensity than that of the 2/98 blend.

It is interesting to note that immediately after shear, the scattered intensity of the shish decreased first ($t < 400$ s) in both blends, which suggests that the volume fraction of the shish or the density contrast between the shish and the surrounding matrix in the blend began to decrease (although the latter may be less likely). It is conceivable that the initial shish entity does not contain purely crystalline structure, where the process of crystallization can reduce the internal force and relax some stretched chains, leading to the reduction of the total scattering volume. This can be further explained as follows. The formation of the initial shish is directly related to the deformation of a network of highly entangled chains, where the entanglement points may be embedded in the shish. Upon crystallization of some oriented and extended chain segments, the internal stress on the network will be reduced, leading to the relaxation of stretched chains in the vicinity of extended-chain crystalline shish. Recently, Olmsted et al. have proposed another possibility, i.e., the interplay between strain and nematic-like orientational interactions of stretched density and orientation fluctuations along the flow axis.[22] In both blends, the scattered intensity of the shish was found to increase at $t > 400$ s. This can be explained by the growth of extended shish, using the concept of autocatalytic process by Peterman et al.[29,30] This will be discussed later. We believe that the final shish structure developed at $t > 2500$ s contained mainly extended-chain crystals, which would be consistent with the WAXD results.

In order to investigate the time-evolution of the shish structure, the changes of the average shish length, $\langle L_{shish}\rangle$, and the misorientation of shish, B_ϕ, were followed. These parameters were obtained by using the Ruland streak method to analyze the equatorial streak feature in SAXS.[31–33] Ruland demonstrated that the size and orientation distributions of longitudinal voids in polymer and carbon fibers in real space could be estimated from the equatorial streak of SAXS in reciprocal space (as long as the orientation and the longitudinal length of scatterer are finite). Since the method is principally based on the separation of experimentally measured azimuthal breadth from contributions of scatterer length and misorientation, the method can also be applied to separate the average length of shish and its average misorientation. If one assumes that all azimuthal distributions can be modeled by Lorentz functions, the observed azimuthal width, B_{obs}, can be related to the length of shish, $\langle L_{shish}\rangle$, and the azimuthal width, B_ϕ, due to misorientation of shish by the following equation.

$$B_{obs} = \frac{1}{\langle L_{shish}\rangle s_{12}} + B_\phi \quad \text{(Cauchy−Cauchy)} \qquad (1)$$

If all azimuthal distributions have Gaussian expressions, then the relationship becomes

$$B_{obs}^{\,2} = \left(\frac{1}{\langle L_{shish}\rangle s_{12}}\right)^2 + B_\phi^{\,2} \quad \text{(Gaussian−Gaussian)} \qquad (2)$$

where B_{obs} represents the integral width of the azimuthal profile from the equatorial streak at s_{12} (the scattering vector $s_{12} =$

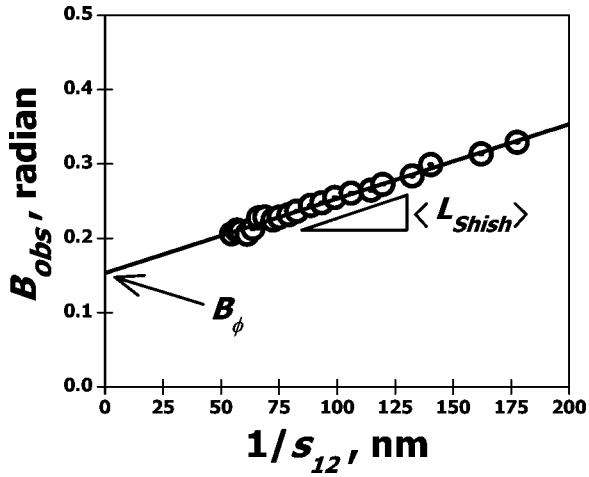

Figure 4. Plot of azimuthal integral width (B_{obs}) vs the value of $1/s$, which was used to determine the average shish length ($\langle \mathbf{L}_{shish} \rangle$) and the shish misorientation (B_ϕ) based on eq 1.

$(s_1^2 + s_2^2)^{1/2} = 2(\sin\theta)/\lambda$). On the basis of eq 1 or eq 2, $\langle L_{shish} \rangle$ can be obtained from the slope, and the misorientation width, B_ϕ can be obtained from the intercept of the plots (B_{obs} vs s_{12}^{-1} or B_{obs}^2 vs s_{12}^{-2}). In this study, we found that all azimuthal distributions were better fit with Lorentz functions, thus the plot based on eq 1 (as shown in Figure 4) was used to determine $\langle L_{shish} \rangle$ and B_ϕ.

In addition, the change of the shish cross-section radius, R_C, was examined by analyzing the equatorial streak profile using the Guinier law for rod-like scatterer.[34] According to this law, the scattered intensity of long rod-like scatterer with length, H and the rod radius, R_C, (where $H \gg R_C$) can be expressed as

$$I(s) = I_H(s)I_C(s) \cong H\frac{1}{2s}(\Delta\rho)^2A^2\exp(-2\pi^2R_C^2s^2) \qquad (3)$$

where the scattered intensities, $I_H(s)$ and $I_C(s)$ are related to the length and the cross-section area of rod-like scatterer, respectively. They are given as follows:

$$I_H(s) \cong H\frac{1}{2s} \qquad (4)$$

$$I_C(s) \cong (\Delta\rho)^2A^2\exp(-2\pi^2R_Cs^2) \qquad (5)$$

where A represents the cross-section area of the rodlike scatterer. Then R_C can be obtained by fitting the linear portion of the ln $I(s)$ vs s^2 plot at the low s region of the curve (i.e., the minimum s is equal to 0.0056), where the intensity $I(s)$ was integrated at $\phi = 0-180°$. It should be noted that the Guinier approximation is applicable for monodisperse systems when $qR_C < 1$.

The time-evolution of two structure parameters of shish ($\langle L_{shish} \rangle$ and $B\phi$, obtained by the Ruland's streak analysis using eq 1 for both blends is shown in Figure 5, parts a and b. The corresponding change of the shish diameter (R_C), obtained by the Guinier analysis, is shown in Figure 6. In Figure 5, the value of $\langle L_{shish} \rangle$ in the 2/98 blend was found to decrease at $t > \sim 400$ s, while the shish orientation increased (i.e., B_ϕ decreased). The decrease in $\langle L_{shish} \rangle$ and the increase in shish orientation can be explained by the partial relaxation of the stretched UHMWPE chain network after shear, where some defective and less oriented shish crystals may melt due to entropic recovery of the stretched chains. It was interesting to see that in the 2/98 blend, $\langle L_{shish} \rangle$ began to increase at $t < 400$ s, accompanying by a decrease in the shish orientation. The increases in the shish length can be attributed to the growth of shish, while the decreases in shish orientation suggests that the growth process took place in stretched chain segments that were partially relaxed (thus resulting in decreasing orientation). Figure 6 indicates that

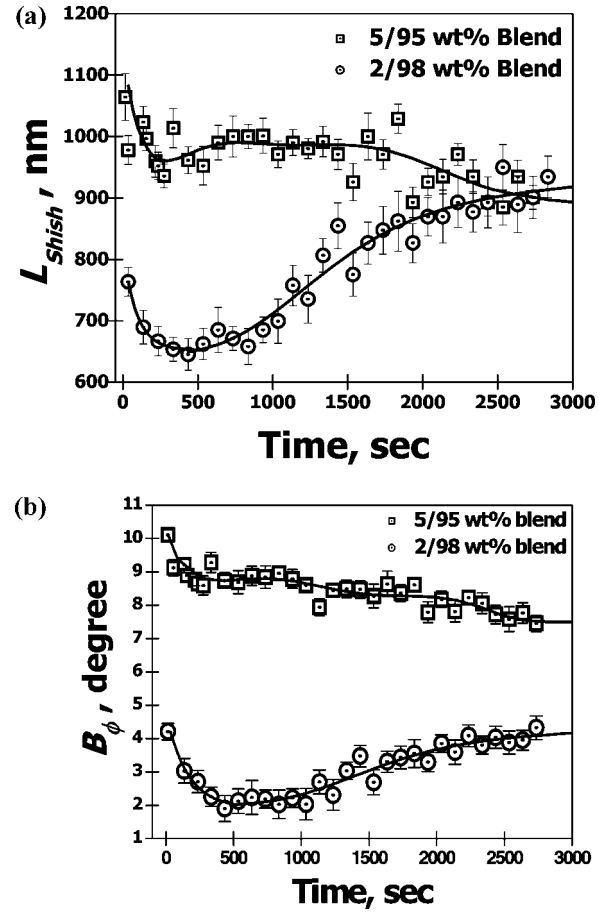

Figure 5. Changes of (a) average shish length ($\langle L_{shish} \rangle$) and (b) shish misorientation (B_ϕ) for each blend obtained immediately after shear at 142 °C ($\dot{\gamma} = 100$ s^{-1} and $t_s = 5$ s).

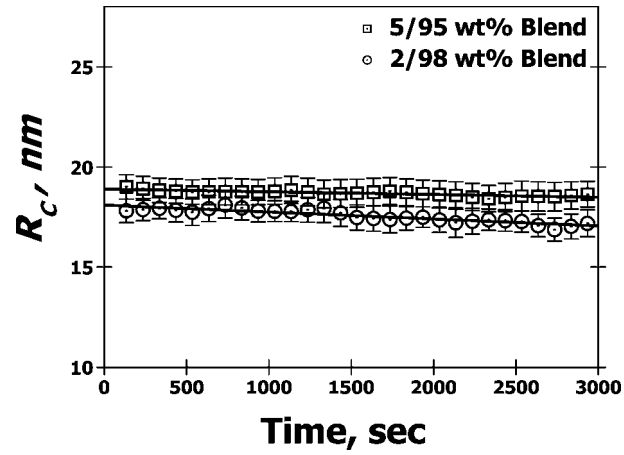

Figure 6. Changes of the shish diameter (R_C) for each blend (R_C was obtained from the Guinier plot, ln $I(s)$ vs s^2, based on eq 3).

the shish diameter (R_C) remained almost about constant with time (a very slight decrease was seen). Keller et al.[29] and Petermann et al.[30] reported that the shish can undergo longitudinal growth in deformed polymer solution, where the growth process is accomplished by preoriented (mesomorphic) chains. The driving force for the longitudinal growth of shish can be attributed to the free energy difference between the formation of shish and the relaxation of stretched "mesomorphic" melts. They argued that if the growth rate of the shish is relatively slow with respect to the relaxation time of the stretched chains, the local orientation of newly formed shish would be reduced. Our results in the 2/98 wt % UHMWPE/HDPE blend are

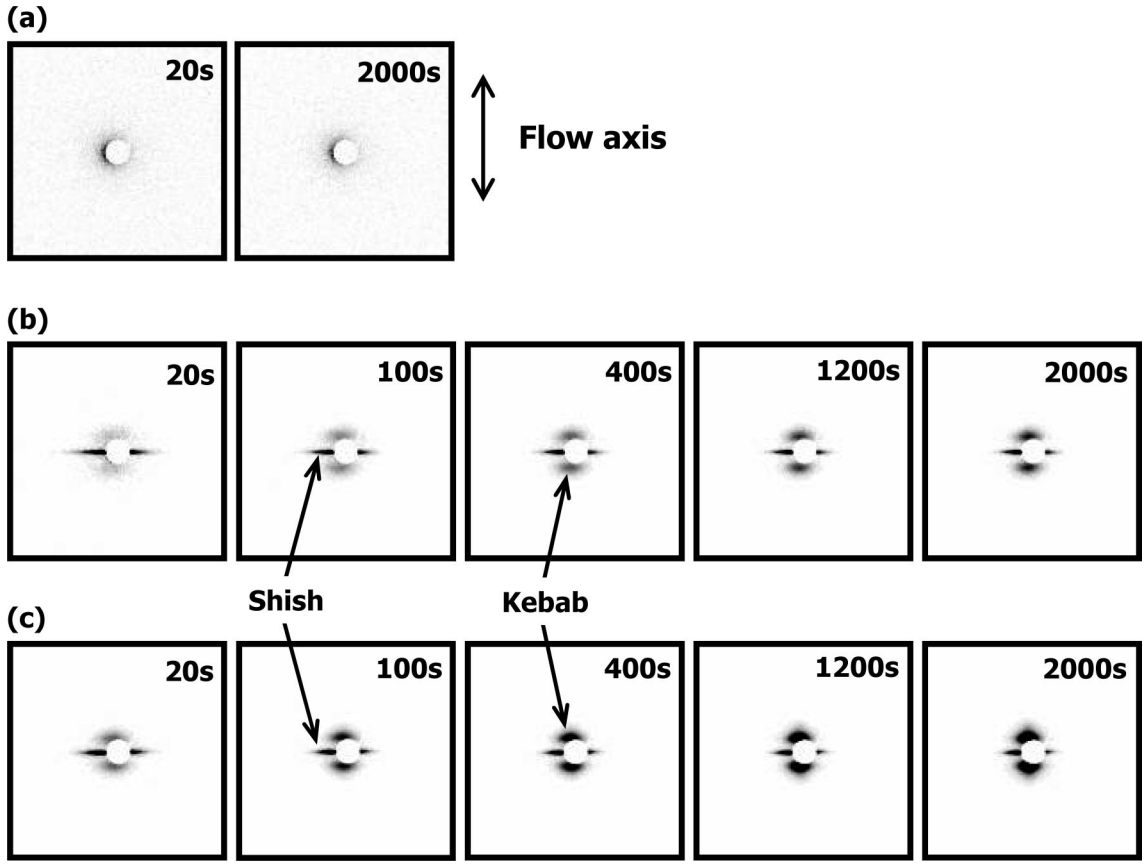

Figure 7. Selected SAXS patterns of once-sheared (a) neat HDPE, (b) 2/98 wt % UHMWPE/HDPE blend, and (c) 5/95 wt % UHMWPE/HDPE blend, collected after rapid cooling from 142 to 134 °C. Prior to the measurement, the melts were sheared at 142 °C ($\dot{\gamma} = 100\ s^{-1}$ and $t_s = 5$ s) and held isothermally for 45 min.

certainly consistent with the mechanism proposed by Keller et al.[29] and Petermann et al.[30]

The behavior of the 5/95 blend was slightly different from that of the 2/98 blend. Although the value of $\langle L_{shish} \rangle$ decreased and the shish orientation increased (i.e., B_ϕ decreased) in the initial stage, these values also exhibited the same trend at the late stage (except at the intermediate stage where both $\langle L_{shish} \rangle$ and B_ϕ decreased). In general, the starting values of $\langle L_{shish} \rangle$ and B_ϕ were higher in the 5/95 blend than those of the 2/98 blend, indicating the latter formed a network of shorter but more oriented shish. This is consistent with our earlier concept[21] that the flow-induced shish-kebab precursor structure comes mainly from the entangled chains of high molecular weights (e.g., UHMWPE). In the lower concentration blend (2/98 wt % UHMWPE/HDPE), the UHMWPE chains are less entangled, forming a lose network with a fewer number of "cross-linking" (entanglement) points. In the higher concentration blend (5/95 wt % UHMWPE/HDPE), the UHMWPE chains are more entangled, resulting in a dense network with more "physical cross-linking" (entanglement) points. Consequently, under the same shear conditions (i.e., $\dot{\gamma} = 100\ s^{-1}$, $t_s = 5$ s and the strain unit $\gamma_s = 500$), the loosely entangled network could be oriented more (due to the smaller modulus) but formed shorter shish length (due to lower concentration), whereas the dense entangled network could be oriented less (due to the higher modulus) but led to longer shish length (due to higher concentration). It is interesting to see that although both blends exhibited the growth process of shish in the intermediate stage, the growth behavior in the higher concentration blend (5/95 wt % UHMWPE/HDPE) was much weaker and lasted for a shorter period of time than that in the lower concentration blend (2/98 wt % UHMWPE/HDPE). This behavior is certainly consistent with the concept of flow-induced network structure containing shish-kebabs from the highly entangled UHMWPE species. It is also interesting to note that in Figure 5a, the shish length became nearly identical (i.e., $\langle L_{shish} \rangle \approx 950$ nm) at the late stage of the shish-kebab formation ($t \approx 2500$ s). Perhaps, this is because the final shish length is thermodynamically dependent (rather than dynamically dependent), which should be the same at the same crystallization temperature.

During the shish-kebab formation, the R_C values for both blends were found to decrease very slightly (Figure 6). The negative slope indicates that the later formed shish probably had a thinner average diameter, which is consistent with the relaxation of stretched chains decreasing the amount of stretched chains that can participate in the shish growth. It is interesting to see that the 5/95 blend generally exhibited a larger R_C value than the 2/98 blend. This also agrees with the notion that as the concentration of the UHMWPE component increases, more UHMWPE chains can be involved in the shish formation leading to a larger R_C value. However, since the difference in R_C between the two blends is small, this indicates that the concentration of UHMWPE is not a strong factor affecting R_C. Instead, the concentration of UHMWPE seems to be a dominant factor affecting the number (concentration) of shish.

Subsequent Kebab Formation at $T_c = 134$ °C. After being held at 142 °C for 45 min, the once-sheared melts were rapidly cooled to 134 °C (at a −30 °C/min rate) to investigate the subsequent crystallization (mainly from the kebab growth). Selected 2D SAXS patterns obtained from the samples immediately after reaching 134 °C are shown in Figure 7. Again, the sheared HDPE melt only exhibited the diffused scattering feature, confirming that the matrix was in the molten state at 134 °C without ordered structure and orientation. In both blends,

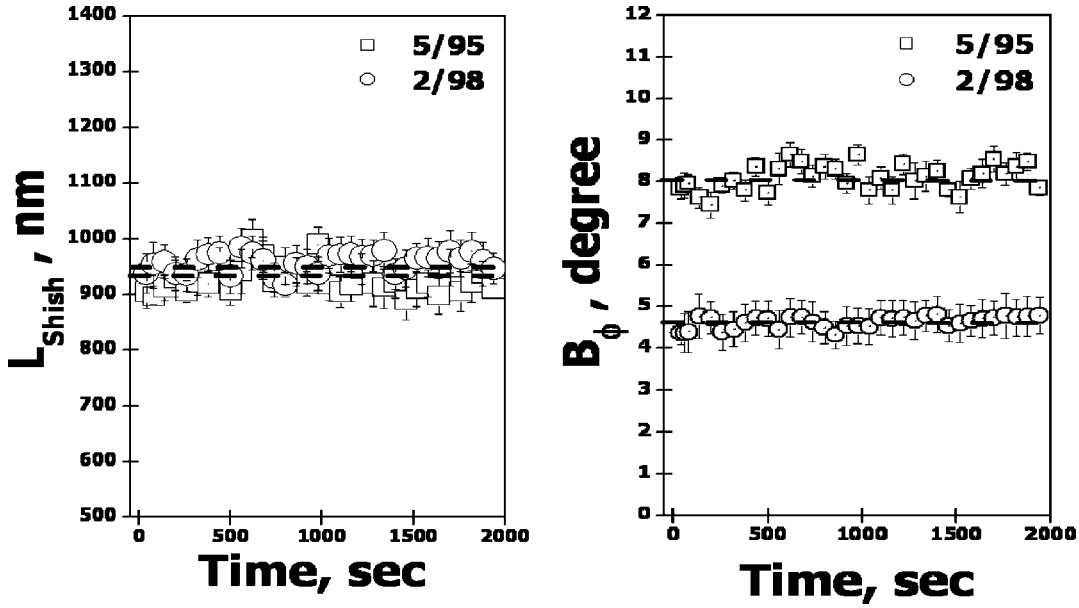

Figure 8. Changes of (a) shish length ($\langle L_{shish} \rangle$) and (b) shish misorientation (B_ϕ) for each blend at 134 °C (results were obtained from Figure 7, parts b and c).

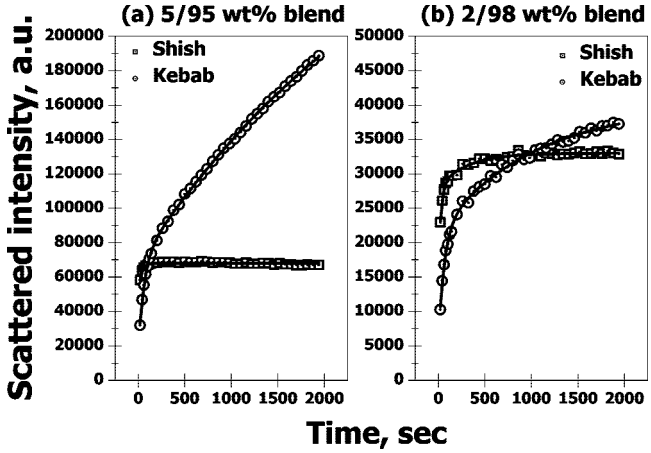

Figure 9. Changes of the scattered intensities from shish and kebabs in (a) 5/95 blend and (b) 2/98 blend (results were obtained from Figure 7, parts b and c).

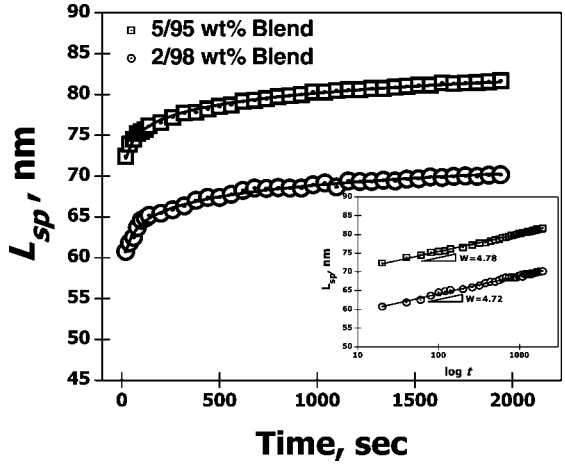

Figure 10. Changes of the kebab long period ($\mathbf{L}_{sp}$) for each blend (the results were obtained from Figure 7, parts b and c). The inset diagram was drawn based on eq 6.

however, SAXS patterns clearly showed the emergence of two meridional scattering maxima due to the kebab formation. This is because the kebabs grow perpendicularly to the shish axis through the folded-chain crystallization process. The layered kebab structure can be considered as the initial template for the formation of lamellar stacks. During the crystallization at 134 °C, the shish lengths and the shish orientations for each blend were almost constant as seen in Figure 8, parts a and b. Furthermore, these values were identical to those observed at the final stages of crystallization at 142 °C (Figure 5, parts a and b). This suggests that the crystallization at 134 °C was mainly due to the kebab growth, where the shish structure became nearly stablized.

To follow the evolution of the kebab growth as well as the further change of shish at 134 °C, scattered intensities from shish and kebabs were separated from the SAXS patterns for both blends (Figure 7, parts b and c), and the results are illustrated in Figures 9(a) and 9(b) respectively. The scattered intensities from shish and kebabs were integrated using the following expressions:

$$I_{\text{shish}} = 4\pi \int_{0.0087}^{0.31} \int_{0^\circ}^{20^\circ} I(s,\phi)\, \mathrm{d}s\, \mathrm{d}\phi \qquad (0)$$

and

$$I_{\text{kebab}} = 4\pi \int_{0.0087}^{0.31} \int_{20^\circ}^{90^\circ} I(s,\phi)\, \mathrm{d}s\, \mathrm{d}\phi \qquad (0)$$

It was seen that the intensities of shish and kebabs increased rapidly at the initial stage in both blends, while such increases slowed down at later times. Since the average shish length in each blend remained almost constant at 134 °C (Figure 8a), the initial increase of the scattered intensity by shish is probably due to the increase in density contrast, $\Delta\rho$, between the shish and the surrounding matrix during subsequent crystallization at lower temperature.

The emergence of meridianal scattering was due to the kebab growth. In Figure 9, the 5/95 blend showed stronger total scattered intensity than the 2/98 blend during entire crystallization stages (note that the unit scale in 5/95 wt % is much higher than that in 2/98 wt %). Since the 5/95 blend possessed a higher concentration of shish (thus a higher number of nucleation site) than the 2/98 blend, the former should result in a higher volume fraction of coiled chains for forming kebabs. The number of kebabs is associated with the nucleation density on the shish; the growth of the kebab is associated with the diffusion of the

Table 1. Nucleation Density of Kebab for the UHMEPE/HDPE Blend

	2/98 wt % UHMWPE/HDPE blend	5/95 wt % UHMWPE/HDPE blend
nucleation density per shish (I)	15.2	12.4

coiled segments onto the shish. It is conceivable that the growth rate of kebabs (diffusion controlled) is not the same as the growth rate of spherulites in transcrystallization, which is a combination of nucleation and growth.

Figure 10 shows the changes of long period (L_{sp}) in the kebab assembly for each blend determined from the 2D rheo-SAXS patterns in Figure 7. This long period represents the sum of the kebab thickness, L_c and the amorphous thickness between the kebabs, L_a; $L_{sp} = L_c + L_a$. It is seen that the kebab long period increased rapidly in the initial stages and slowed down at later times. In the past, the increase of kebab long period has been attributed to the surface melting of kebab crystals and the subsequent recrystallization to form more stable and thicker crystals.[35–37] This can also be the case here. The stability of kekab crystals (folded-chain lamellae) is related to the ratio of bulk free energy (σ) and surface free energy (μ), σ/μ. When the crystal thickens, the σ/μ ratio increases and the crystal stability is enhanced. One often observes such a phoenomenon at crystallization temperature near the melting point, T_m, where large chain mobility permits small crystals to melt and large crystals to thicken to a more stable state. Petermann demonstrated that the rate of crystal thickening increases with crystallization temperature, T_c, by the following equations:[36]

$$L_{sp}(t) = W \log t + p \tag{6}$$

where, W is the rate of crystal thickening and p is a constant. The inset in Figure 10 shows the plot of $L_{sp}(t)$ versus log t, where the rates of crystal thickening for two blends are almost identical. This is reasonable since the rate of thickening is mainly dependent on crystallization temperature, not chain entanglement or flow condition. This also implies that the growth of kebabs in two different blends takes place mainly in the coiled segments of UHMWPE, which has the same diffusion rate thus resulting in the same thickening rate.

It is interesting to note that the kebab long period in the 2/98 blend was less (Figure 10) than that in the 5/95 blend at the same crystallization temperature. This has the following implication. Earlier, we observed that the 5/95 blend possessed a higher concentration of shish (thus a higher number of nucleation site) than the 2/98 blend, the total number of nucleated kebabs thus would also be higher in the 5/95 blend. Since both L_{shish} and L_{sp} values are known, the nucleation density of kebabs per shish, I, can be calculated by the ratio of L_{shish}/L_{sp} (the result was listed in Table 1). It is seen that the nucleation density of kebab per shish was higher in the 2/98 blend than in the 5/95 blend. In other words, the nucleation density per shish decreased as the concentration of shish increased. This phoenomenon has also been observed in our previous studies, but it was not reported. The behavior is associated with the respective concentrations of nucleating shish and surrounding crystallizable coiled chains. A simple scenario one can conclude is that the 2/98 blend contained more crystallizable coiled chains surrounding the shish, whereas the 5/95 blend possessed more shish with less crystallizable coiled chains surrounding the shish. This is possible as the 5/95 blend may form a dense shish network, where more UHMWPE chains are under strained conditions. As the amount of crystallizable coiled chains surrounding the shish is higher in the 2/98 blend than the 5/95 blend, the former would result in a higher nucleation density per unit shish as seen experimentally.

Selected rheo-2D WAXD patterns collected during crystallization in the sheared melts (neat HDPE and UHMWPE/HDPE blends) at 134 °C are shown in Figure 11, parts a−c, respectively. These rheo-2D WAXD patterns were obtained under the same condition as rheo-2D SAXS patterns in Figure 7, parts a−c. It was seen that WAXD patterns of the once-sheared HDPE sample exhibited no sign of crystallization at 134 °C. In contrast, WAXD patterns of both sheared blends exhibited 2-bar oriented (110) reflections on the equator at the initial times (e.g., 20 s) and the superposition of weak but discernible 2-arc (110) reflections around the equator with increasing time (e.g., 400 s). The 2-bar equatorial (110) reflections can be attributed to the extended-chain UHMWPE crystals (shish) formed at 142 °C, while the broad 2-arc equatorial (110) reflections can be attributed to the folded-chain UHMWPE crystals (kebabs) formed at 134 °C. It was interesting to see that the 2-arc (110) reflections gradually transforms into 4-arc off-axis (110) reflections at the later time. The off-axis (110) reflections are associated with the formation of twisted kebabs. This can be explained as follows. The transformation of (110) reflections from equatorial 2-arc to off-axis 4-arc features is due to the rotation of reciprocal lattice vector, r_{110}*, from the step of initiation to twisting during kebab growth. In the transformation, both *a*- and *c*-axes rotate along the *b*-axis, resulting in the turning of r_{110}* along the azimuthal angle, which leads to first broadening and eventually off-axis splitting of (110) reflections.[20,39]

Changes of the (110) reflection intensities from shish and kebabs for each blend are illustrated in Figure 12 (results were obtained from Figure 11, parts b and c, where the (110) reflections by shish and kebabs are indicated). The separation of the (110) reflections from shish and kebab was carried out by curve-fitting of the integrated azimuthal profiles using Gaussian functions. However, prior to this process, the following procedures were applied first. To correct the missing intensity due to the use of flat-plate detector, the measured intensity at given scattering vector and azimuthal angle, $I_{110}(s, \phi)$, was multiplied by a correction factor, $s^2 \sin(90 - \phi)$.[34,38] Thus, the total integrated intensity of the (110) reflection can be given as: $I_{110,T}(s, \phi) = I_{110,S}(s, \phi) + I_{110,K}(s, \phi)$, where $I_{110,S}(s, \phi)$ represents the integrated intensity from shish and $I_{110,K}(s, \phi)$ represents the integrated intensity from kebabs. In addition, the following relationship also holds:

$$I_{110,T}(s, \phi) = 4\pi \int_0^\infty s^2 \, ds \int_0^{\pi/2} \sin(90° - \phi) \, d\phi \, I(s, \phi) \tag{0}$$

Since the kebab intensity is proportional to the volume fraction of kebabs or folded chain crystals (V), $I_{110,K}(t) \alpha V(t)$, the time-dependence of the kebab intensity may directly reflect the time-evolution of kebab volume, especially at the initial stage of crystallization. As a result, a simplified Avrami equation[39] was used to analyze the kebab intensity to investigate the nucleation and growth of kebabs.

The general Avrami equation (eq 7) has been routinely used to study the crystallization kinetics of polymers.[40]

$$v_c = 1 - \exp(-Kt^n) \tag{7}$$

Since the volume fraction of crystal attained is less than 1, the general Avrami equation for polymer crystallization can be expressed as follows.[41]

$$\frac{v_c(t)}{v_c(\infty)} = 1 - \exp(-Kt^n) \tag{8}$$

where $v_c(t)$ and $v_c(\infty)$ are volume fractions of crystal at time t and at infinite time (∞), K is the rate constant and n is the Avrami exponent. The following relationship also holds for X-ray diffraction data, $v_c(t)/v_c(\infty) \propto V \propto I_c(t)/I_c(\infty) \propto I_c(t)$, where

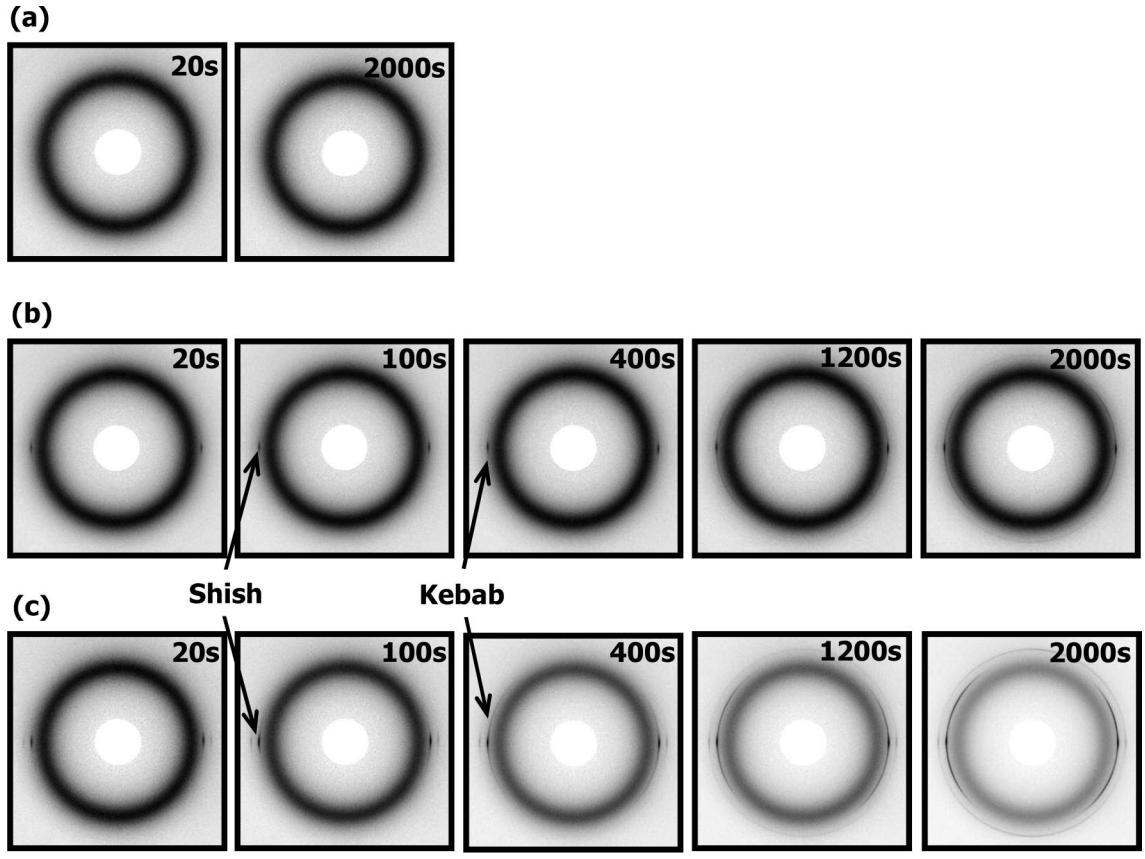

Figure 11. Selected WAXD patterns of once-sheared (a) neat HDPE, (b) 2/98 wt % UHMWPE/HDPE blend, and (c) 5/95 wt % UHMWPE/HDPE blend, collected after rapid cooling from 142 to 134 °C. Prior to the measurement, the melts were sheared at 142 °C ($\dot{\gamma} = 100\ s^{-1}$ and $t = 5$ s) and held isothermally for 45 min.

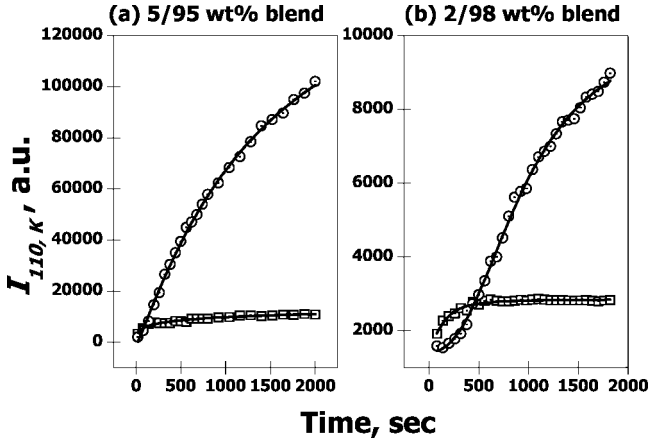

Figure 12. Changes of the (110) reflection intensities from shish and kebabs for each blend (results were obtained from Figure 11, parts b and c).

$I_c(t)$ and $I_c(\infty)$ are diffraction intensities of crystal at time t and infinite time (∞). Since the expression $\exp(-Kt^n) \approx 1 - Kt^n + \ldots$, one can simplify the Avrami expression as follows:[39–41]

$$I_c(t) \sim kt^n \tag{9}$$

or

$$\log I_c(t) \sim \log k + n \log t \tag{10}$$

Thus, from the changes in the (110) intensity at the initial stages of crystallization, the Avrami exponents, n, and the constant, k (which is related to the rate constant, K) can be obtained from the simplified Avrami plot as shown in Figure 13. The Avrami exponent n and the constant k obtained from such analysis are listed in Table 2. It is seen that the estimated Avrami exponents at the initial stage of kebab formation for each blend are about

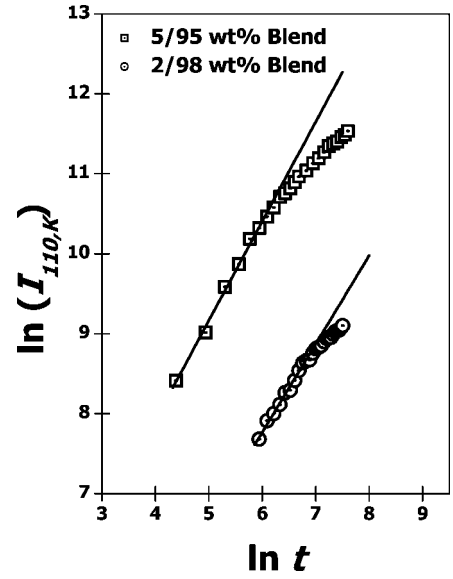

Figure 13. Simplified Avrami plot (eq 10) for the kebab formation (based on the (110) reflection intensity) for each blend (results were obtained from Figure 11, parts b and c).

Table 2. Avrami Exponent, n, and the Constant, k (Related to Avrami Rate Constant, K) of the UHMWPE/HDPE Blend

n	1.1	1.2
k	3.1	19.1

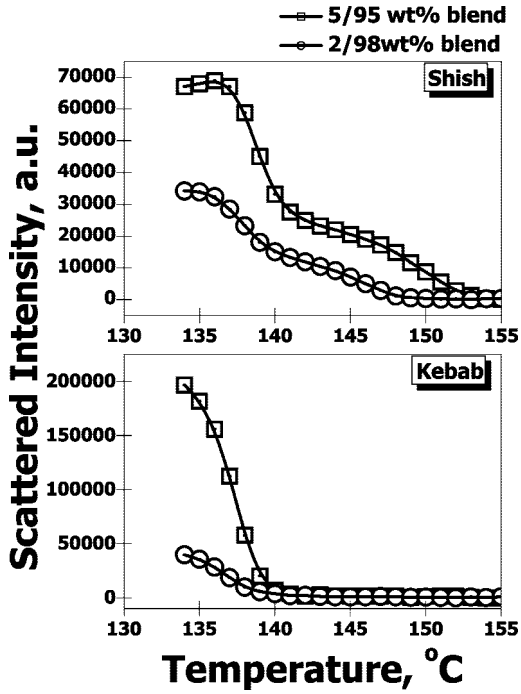

Figure 14. Changes of the scattered intensities from shish and kebab for each blend upon subsequent melting (the once-sheared sample was crystallized at 142 and 134 °C).

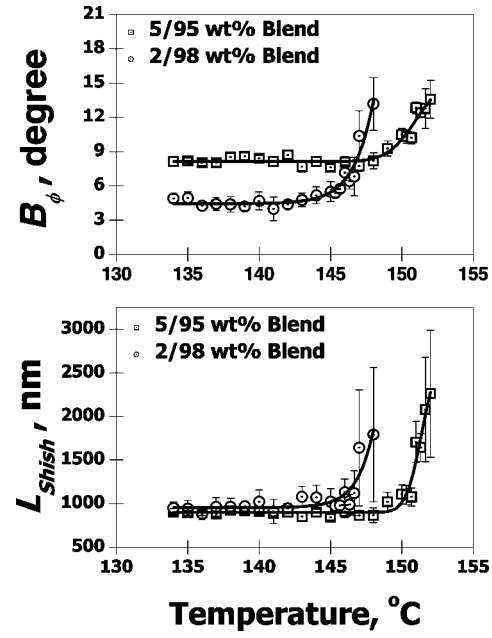

Figure 15. Changes of the shish length ($\langle L_{shish} \rangle$) and shish misorientation (B_ϕ) for each blend upon subsequent melting (the once-sheared sample was crystallized at 142 and 134 °C).

the same ($n \approx 1$), which indicates the kebabs following the 2D growth geometry under athermal (spontaneous) nucleation and diffusion-controlled crystallization conditions.[41,42] Since the constant k is related to the crystallization rate, the results imply that the kinetic of kebab growth was much faster in 5/95 blend than in 2/98 blend under the same crystallization conditions. If the nucleation process and the growth geometry of kebabs are predetermined, the kebab growth rate (i.e., the y-intercept in Figure 13) is governed by the number of nucleation site. Even though the average number of the kebab nucleation density per shish is higher in the 2/98 blend than that in the 5/95 blend as seen in Table 1, the higher crystallization rate of the 5/95 blend implies that the total number of nucleation is also higher in the 5/95 blend. This is consistent with the experimental observations.

Probing the Stability of Shish-Kebab Structure in Once-Sheared Melts by Confined Melting. The stability of shish (formed at 142 °C) and kebabs (formed at 134 °C) in once-sheared melts was examined by confined melting using the following procedures. The flow-induced crystallized samples were heated at 1 °C/min under the planar constraint conditions in the Linkam shear device. The changes of scattered intensities by shish and kebabs in each blend upon melting are illustrated in Figure 14. Both blends exhibited total melting of kebabs at about the same temperature ($T_m \approx 140$ °C), which implies that the isothermal crystallization of two sheared blends with different UHMWPE concentrations at 134 °C formed kebabs of an identical thickness distribution. In other words, although the kebab development can be mediated and prompted by shearing of different blends, the kebab growth in both systems follows the thermodynamics of crystallization. In our previous study, we reported that the equilibrium melting temperature of polyethylene (PE) folded-chain crystals (kebabs) obtained from constrained melting of sheared sample was $T°_m \approx 142.6$ °C.[43] Even though this value is lower than the theoretical value of equilibrium melting temperature for PE, $T°_m \approx 145.5$ °C, the estimated value in this study is in good agreement with the experimental data determined by Wunderlich,[5] $T°_m \approx 141.5$ °C (in their study, the lamellae were formed under an equilibrium condition in the absence of flow, and the melting was proceeded without constraint). The above observations clearly indicated that the crystallization and melting of kebabs are governed by thermodynamics as unstrained or nonsheared melts.

In Figure 14, the melting of shish for the two blends exhibited two stages: the initial melting at $T \leq 140$ °C, where the temperature range was identical to that of kebabs observed earlier; and the later melting at $T \geq 140$ °C. The two-stage melting behavior in shish can be understood by the following experimental observations. Figure 15 illustrates changes of shish length and shish orientation, which were about constant at $T \geq 140$ °C. The initial decrease of scattered intensity in Figure 14 are probably associated with the decrease of packing density in extended-chain crystals and thus leads to the decrease in density difference (scattering contrast), $\Delta\rho$, between the shish and surrounding molten matrix. It is interesting to note that the melting points of shish for both blends were higher than the theoretical equilibrium melting temperature (145.5 °C). This may be explained as follows. Different from kebabs, the growth and melting of shish in both blends are dominated by nonequilibrium factors, imposed by stretched chains and entanglement network. Since the dimension of sample was confined under planar constrained condition during crystallization and melting, the stretched chain could not freely relax upon melting. As a result, the nominal melting point of shish increased to a level higher than the equilibrium melting temperature, (145.5 °C). This has also been observed in two UHMWPE systems: (1) extended-chain crystals of drawn UHMWPE fibers, which shows an increased melting temperature higher than the equilibrium melting temperature; (2) the phase transition from orthorhombic to hexagonal phase in oriented UHMWPE, where the transition temperature is also higher than the equilibrium melting temperature.[44,45]

Even though the external constraint applied to the sheared melts was constant and the observed structure parameters, such as the shish length, is about the same in both blends, the nominal shish melting temperature in 5/95 blend was higher than that in 2/98 blend (i.e., 153 °C vs 148 °C in Figure 15). This may be explained as follows. The melting of shish is accompanied by the topological relaxation of stretched UHMWPE chains in the entanglement network (the total number of entanglement is

higher in 5/95 blend than 2/98blend due to the concentration effect). We note that the chain entanglement is a dynamic process which forms and disappears. In the supercooled state, when the chain dynamics are slow, one may assume the entangled melt behaves as a physical network. The shear deformation would generate two populations of UHMWPE chain segments with different orientations: (1) stretched chain segments, which are oriented along the flow direction and are confined by the "frozen" entanglement points, and (2) unperturbed chain segments (or coiled segments).[12] As a result, only a fraction of UHMWPE can be oriented by flow and participate in the shish formation, while others remain in the unperturbed state but they are connected to and surround the shish. Since the total number of entanglement in the 5/95 blend is higher than that in the 2/98 blend, the former has a higher thermal stability. This is seen in Figure 15, where both blends exhibit the increase in shish length and the decrease in shish orientation (the higher B_ϕ value, the higher shish misorientation) with the 5/95 blend having higher thermal stability. It is interesting to see that the average shish lengths for both blends were about the same, but the 5/95 blend exhibited a higher shish misorientation, probably due to the stronger entanglement network that would recoil faster upon stress relaxation.

Conclusions

In situ rheo-SAXS and rheo-WAXD studies were carried out to investigate flow-induced crystallization of UHMWPE/HDPE blends, where UHMWPE chains (with long relaxation times) play the major role in forming the entanglement network. The combined SAXS and WAXD results confirmed that the shear-induced shish formation at 142 °C was mainly originated from UHMWPE chains. The final shish lengths in two blends (2/98 wt % and 5/95 wt %) were about the same within the experimental error, even though the UHMWPE compositions were quite different. The identical shish length in these two blends might be due to the identical strain ($\epsilon = 500$) imposed on the supercooled and restrained melts. As the temperature decreased to 134 °C, both blends exhibited the formation of kebabs, where growth process was diffusion-controlled rather than nucleation-controlled. Even though the total nucleation number of kebab was higher in the 5/95 blend, the nucleation density of kebab per unit shish was higher in the 2/98 blend. This could be attributed to the different concentrations of shish and crystallizable coiled chains in the sheared melts. The once-sheared (at 142 °C) and crystallized (at 134 °C) samples were subject to subsequent heating under planar constraint to investigate the thermal stability of shish-kebab structure. Both blends exhibited an identical melting temperature of kebabs, indicating that the kebab stability is dictated by the thermodynamics of coiled chains. In contrast, the high melting temperature of shish indicates that the shish stability is dictated mainly by the thermodynamics of stretched chains under the planar constrained conditions.

Acknowledgment. We acknowledge the assistance of Drs. Igors Sics and Lixia Rong for synchrotron SAXS and WAXD experimental setup. The financial support of this work was provided by National Science Foundation (DMR-0405432) with a special creativity extension award.

References and Notes

(1) Keller, A. *Faraday Discuss. R. Chem. Soc.* **1979**, *68*, 145.
(2) Hill, M. J.; Keller, A. *J. Macromol Sci. (Phys.)* **1969**, *B3*, 1531.
(3) Keller, A.; Kolnaar, H. W. *Mater. Sci. Technol.* **1997**, *18*, 189.
(4) Ward, I. M. *Structure and Properties of Oriented Polymers*; Wiley: New York, 1975.
(5) Wunderlich, B. *Macromolecular Physics*; Academic Press: New York 1973; Vol. *2*.
(6) Wilkinson, A. N., Ryan, A. J., Eds.; *Polymer Processing and Structure Development*; Kluwer: Dordrecht, The Netherlands, 1998.
(7) Pennings, A. J.; Kiel, A. M. *Colloid. Z. Z. Polym.* **1965**, *205*, 160.
(8) Nadkarni, V. M.; Schultz, J. M. *J. Polym. Sci. Phys. Ed.* **1977**, *15*, 2151.
(9) Dukovski, I.; Muthukumar, M. *J. Chem. Phys.* **2003**, *118*, 6648.
(10) Hsiao, B. S.; Yang, L.; Somani, R. H.; Carlos, A. A.; Zhu, L. *Phys. Rev. Lett.* **2005**, *94*, 117802.
(11) Keum, J. K.; Burger, C.; Hsiao, B. S.; Somani, R. H.; Yang, L.; Chu, B.; Kolb, R.; Chen, H.; Lue, C. *Prog. Colloid Polym. Sci.* **2005**, *130*, 114.
(12) Zuo, F.; Keum, J. K.; Yang, L.; Somani, R. H.; Hsiao, B. S. *Macromolecules* **2006**, *39*, 2209.
(13) Seki, M.; Thurman, D. W.; Oberhauser, J. P.; Kornfield, J. A. *Macromolecules* **2002**, *35*, 2583.
(14) Somani, R. H.; Hsiao, B. S.; Nogales, A.; Srinivas, S.; Tsou, A. H.; Sics, I.; Balta Calleja, F. J.; Ezquerra, T. A. *Macromolecules* **2000**, *33*, 9385.
(15) Jerschow, P.; Janeschitz-Kriegl, H. *Int. Polym. Process.* **1997**, *12*, 72.
(16) Vleeshouwers, S.; Meijer, H. *Rheol. Acta* **1996**, *35*, 391.
(17) Duplay, C.; Monasse, B.; Haudin, J. M.; Costa, J. L. *J. Mater. Sci.* **2000**, *35*, 6093.
(18) de Gennes, P. G. *J. Chem. Phys.* **1974**, *60*, 5030.
(19) Schroeder, C. M.; Babcock, H. P.; Shaqfeh, E. S. G.; Chu, S. *Science* **2003**, *301*, 1515.
(20) Kolnaar, J. W. H.; Keller, A. *Prog Colloid Polym. Sci.* **1993**, *92*, 81.
(21) Yang, L; Somani, R. H.; Sics, I.; Hsiao, B. S.; Kolb, R.; Fruitwala, H.; Ong, C. *Macromolecules* **2004**, *37*, 4845.
(22) Olmsted, P. D.; Milner, S. T. *Macromolecules* **1994**, *27*, 6648.
(23) Murase, H.; Kume, T.; Hashimoto, T.; Ohta, Y. *Macromolecules* **2005**, *38*, 8719.
(24) Olmsted, P. D.; Poon, W. C. K.; McLeish, T. C. B.; Terril, N. J.; Ryan, A. J. *Phys. Rev. Lett.* **1998**, *81*, 373.
(25) Hoffman, J. D.; Lauritzen, J. I. *J. Res. Natl. Bur. Stand.* **1961**, *65A*, 297.
(26) de Gennes, P. G. *Scaling Concepts in Polymer Physics*; Cornell University Press: Ithaca, NY, 1979.
(27) Takahashi, Y.; Isono, Y.; Noda, I.; Nagasawa, M. *Macromolecules* **1985**, *18*, 1002.
(28) Fetters, L. J.; Lohse, D. J.; Garcia-Franco, C. A.; Brant, P.; Richter, D. *Macromolecules* **2002**, *35*, 10096.
(29) Liberwirth, I.; Loos, J.; Petermann, J.; Keller, A. *J. Polym. Sci. Polym. Phys.* **2000**, *38*, 1183.
(30) Petermann, J.; Miles, M.; Gleiter, H. *J. Polym. Sci. Polym. Phys.* **1979**, *17*, 55.
(31) Ruland, W. *J. Polym. Sci., Polym. Symp.* **1969**, *28*, 143.
(32) Ruland, W.; Perret, R. *J. Appl. Crystallogr.* **1969**, *2*, 209.
(33) Ruland, W.; Perret, R. *J. Appl. Crystallogr.* **1970**, *3*, 525.
(34) Guinier, A.; Fournet, G. *Small-angle scattering of X-rays*; Wiley: New York, 1955.
(35) Fisher, E. W.; Schmidt, G. F. *Angew. Chem.* **1962**, *74*, 551.
(36) Peterlin, A. *Macromol. Chem.* **1964**, *74*, 107.
(37) Hikosaka, M.; Amano, K.; Rastogi, S.; Keller, A. *Macromolecules* **1997**, *30*, 2067.
(38) Fraser, R. D. B.; Macrae, T. P.; Miller, A.; Rowlands, R. J. *J. Appl. Crystallogr.* **1976**, *9*, 81.
(39) Keum, J. K.; Burger, C.; Zuo, F.; Hsiao, B. S. *Polymer* **2007**, *48*, 4511.
(40) Avrami, M. J. *Chem. Phys.* **1939**, *7*, 1103.
(41) Gedde, U. W. *Polymer Physics*; Chapman & Hall: New York, 1995..
(42) Hiemenz, P. C. *Polymer Chemistry: The Basic Concepts*; Marcel Dekker: New York, 1984; p 219.
(43) Keum, J. K.; Somani, R. H.; Zuo, F.; Burger, C.; Sics, I.; Hsiao, B. S.; Chen, H.; Kolb, R.; Lue, C. *Macromolecules* **2005**, *38*, 5128.
(44) Bassett, D. C.; Block, S.; Piermarini, G. J. *J. Appl. Phys.* **1974**, *45*, 4146.
(45) Tashiro, K.; Sasaki, S.; Kobayashi, M. *Macromolecules* **1996**, *29*, 7460.

MA800063E